Riemannian metrics for statistics on shapes: Parallel transport and scale invariance

Marc Niethammer[1] and François-Xavier Vialard[2]

[1] UNC Chapel Hill
`mn@cs.unc.edu`
[2] Université Paris-Dauphine, Ceremade UMR CNRS 7534
`vialard@ceremade.dauphine.fr`

Abstract. To be able to statistically compare evolutions of image time-series data requires a method to express these evolutions in a common coordinate system. This requires a mechanism to transport evolutions between coordinate systems: e.g., parallel transport has been used for large-displacement diffeomorphic metric mapping (LDDMM) approaches. A common purpose to study evolutions is to assess local tissue growth or decay as observed in the context of neurodevelopment or neurodegeneration. Hence, preserving this information under transport is important to allow for faithful statistical analysis in the common coordinate system. Most basically, we require scale invariance. Here, we show that a scale invariant metric does not exist in the LDDMM setting. We illustrate the impact of this non-invariance on parallel transport. We also propose a new class of Riemannian metrics on shapes which preserves the variation of a global indicator such as volume under parallel transport.

Keywords: parallel transport, scale invariance, Riemannian metrics on shapes

1 Introduction

Classical image registration deals with the spatial alignment of pairs of images. It is one of the most fundamental problems in medical image analysis. In particular, for population-studies image registration is an indispensable tool, as it allows to align image information to a common coordinate system for localized comparisons. Recently, studies for example on Alzheimer's disease (ADNI), osteoarthritis (OAI), and brain development (NIHPD) have acquired large volumes of longitudinal imaging data. However, computational methods to adequately analyze such longitudinal data are still in their infancy. Analyzing longitudinal image data is challenging: not only is a method for spatial alignment to a common coordinate system required, but also the temporal aspect of a longitudinal image change needs to be expressed in this common coordinate system. Arguably, the theoretically most advanced existing methods to address these problems have been methods grounded in the theory of large-displacement-diffeomorphic metric mapping (LDDMM) [2]. Indeed, LDDMM provides a convenient Riemannian

setting [15] for image registration. Other Riemannian metrics have been developed in the past years [16, 11, 12] sometimes due to the simple calculation of geodesics. Thus, tools from Riemannian geometry can be used to perform statistics on shape deformations [14, 9, 6]. In particular, parallel transport under the Levi-Civita connection gives a method to transport small longitudinal evolutions between two different images. The use of parallel transport in computational anatomy has been introduced in [17], including a numerical method based on Jacobi fields for its computation. Other numerical methods for parallel transport have been successfully developed in [4]. Note that parallel transport is path-dependent. For shapes it has a strong relation to shape correspondence [13] making it a promising candidate to transport longitudinal information. Alternatively, the adjoint [7] and the co-adjoint [3] actions on the tangent space have been proposed to transport tangent information.

In this paper, we show that these methods preserve properties which may be undesirable for computational anatomy. Further, we explore the design of a Riemannian metric conserving quantities such as absolute or relative volume variation. As a case in point, consider Alzheimer's disease where the decay of the hippocampus is an important biomarker. Hence, preserving the relative volume variation when transporting longitudinal change to an analysis space is desirable. However, only specific metrics result in such a parallel transport – volume variations will be distorted under parallel transport using an "unsuitable" metric. In particular, this is the case for LDDMM, which is not scale-invariant.

Sec. 2 illustrates shortcomings of parallel and co-adjoint transport for LDDMM. This is not a shortcoming of a *particular* LDDMM metric, but holds for all as a non-degenerate scale-invariant metric does not exist for LDDMM (see Sec. 3). Consequentially, we introduce a new model decomposing volume and shape variation in Sec. 4 as an example of a Riemannian metric addressing some of the shortcomings of LDDMM. Sec. 5 illustrates behavioral differences between LDDMM and the shape/volume-decomposed model. The paper concludes with a summary of results and an outlook on future work in Sec. 6.

2   Motivating examples

To illustrate the behavior of different types of transport under the LDDMM model we consider a uniformly expanding or contracting n-sphere of radius r, S_n, with uniformly-distributed momentum. Due to the spherical symmetry this allows us to explicitly compute expressions for co-adjoint and parallel transport. Specifically, we define the momentum at radius 1 as $m_1 = c\frac{x}{\|x\|}\delta\{\|x\| - 1\}$, where $c \in \mathbb{R}$ is a given constant and $\delta\{x\}$ denotes the Dirac delta function. Uniform scaling to radius r is described by the map $\Phi^{-1}(x) = \frac{1}{r}x$, which is in the coordinate system of the sphere of radius r. We note that the local volume-change of the n-sphere, $|D\Phi^{-1}|$ with respect to the unit-sphere is given by

$$|D\Phi^{-1}| = \frac{vol(S_n(r))}{vol(S_n(1))} = \left(\frac{1}{r}\right)^d, \tag{1}$$

where d is the space dimension and $vol(S_n(r))$ denotes the volume of $S_n(r)$.

Co-adjoint and parallel transport respectively preserve the dual pairing and the riemannian norm, so that due to the symmetry of momentums and spheres, this property completely determines the transported momentums in both cases. Sec. 2.1 derives the co-adjoint and Sec. 2.2 the parallel transport for this sphere under contraction and expansion. Sec. 2.3 demonstrates their differences.

2.1   Co-adjoint transport

In what follows, n will denote the unit normal to the sphere and v is vector field defined on the whole domain.

Definition: We can define the co-adjoint transport to the momentum-velocity pairing $\langle m_1, v \rangle := \int_{S_n(1)} \langle n, v(x) \rangle \, dS(x)$. Then (with $g^{-1} = \Phi$)

$$\langle Ad_{g^{-1}}{}^*(m_1), v \rangle = \int_{S_n(1)} \langle n, r^{-1}v(rx) \rangle \, dS(x) = \int_{S_n(r)} \langle n, v(y) \rangle r^{-d} \, dS(y). \quad (2)$$

Hence, the co-adjoint transport of the momentum is given by

$$m_r = m_1 \circ \Phi^{-1} |D\Phi^{-1}| = c \frac{\frac{1}{r}x}{\|\frac{1}{r}x\|} \delta\{\|\frac{1}{r}x\| - 1\} \left(\frac{1}{r}\right)^d = c \frac{x}{\|x\|} \delta\{\|x\| - r\} \left(\frac{1}{r}\right)^d.$$

Velocity computation: The velocity is the momentum convolved with kernel K:

$$v_r(x) = K * m_r(x) = \left(\frac{1}{r}\right)^d c \int_{S_n(r)} K(x - y) \frac{y}{\|y\|} \, dS(y). \quad (3)$$

Since we assume a perfectly symmetric distribution it is sufficient to evaluate the velocity at one location on the circle, e.g., at re_1, i.e., we need to compute

$$\tilde{v}_r := v_r(re_1) \cdot e_1 = \left(\frac{1}{r}\right)^d c \underbrace{\int_{S_n(r)} K(re_1 - y)y_1 \, dS}_{:=q(r)} = \frac{cq(r)}{r^d}, \quad (4)$$

where we made use of the fact that $v_r(re_1)$ will only have a velocity component in the e_1 direction due to symmetry and e_1 is the first canonical unit vector.

Note that we computed co-adjoint transport with respect to the uniform scaling map Φ, which is not an element of the diffeomorphisms group since it does not converge to the identity at infinity. Another natural map that could be used for co-adjoint transport is the optimal diffeomorphism obtained by solving the LDDMM functional, but this reduces to parallel transport developed in the next section.

2.2   Parallel transport

The geodesic between the sphere of radius 1 and radius r will possess the same symmetry in its shape evolution. The momentum will also be radial and constant on the sphere. It can also be checked that the parallel transport (along the geodesic) of m_1 to radius r will be λm_r for a real λ that we have to determine. To this end, we use the conservation of the norm under parallel transport, i.e.,

$$\int_{S_n(1)} \langle v_1(x), m_1(x) \rangle \, dS = \int_{S_n(r)} \langle v_r(x), m_r(x) \rangle \, dS. \tag{5}$$

In the e_1 direction we can then write $\tilde{v}_1 \tilde{m}_1 = r^{d-1} \tilde{v}_r \tilde{m}_r$, where $\tilde{m}_r := m_r(re_1) \cdot e_1$. But according to our assumption: $\tilde{m}_r = \lambda \tilde{m}_1$ and we obtain $\tilde{v}_1 = r^{d-1} \lambda \tilde{v}_r$, and $\quad \tilde{v}_r = \lambda cq(r)$, which yields

$$|\lambda| = \sqrt{\frac{\tilde{v}_1}{r^{d-1} cq(r)}} \text{ and finally } \tilde{v}_r = \lambda cq(r) = sign(c) \sqrt{\frac{\tilde{v}_1 cq(r)}{r^{d-1}}} \,. \tag{6}$$

We note that this is up to a multiplicative constant, the square root of the co-adjoint transport. Hence, we can expect a drastically different behavior for the two types of transport.

2.3   Simulations

We solve the equations for parallel (6) and co-adjoint (4) transport numerically for different kernels and different radii. In particular, we use an isotropic Gaussian kernel of the form $K(x) = c_g e^{-\frac{x^T x}{2\sigma^2}}$, where the normalization constant c_g can be subsumed into c (and will therefore be disregarded in what follows). In our experiments we computed all integrations in polar coordinates (2D) and spherical coordinates (3D) respectively. Fig. 1 shows numerical results for S_1 (i.e., the two-dimensional case) for the scaling map. We observe the following:

1) The velocity is kernel-size dependent.
2) Depending on the relation of the size of the object to the kernel-size, velocity may either increase or decrease with increased radius.
3) The radius for which the maximal velocity is obtained roughly coincides with the standard deviation of the Gaussian kernel.
4) The velocity versus radius plots are asymmetric.
5) Velocities converge to zero as $r \to 0^+$ and $r \to \infty$.
6) Parallel transport and co-adjoint transport show similar trends however with different asymptotes for the velocity.

The same conclusions hold in the 3D case, albeit with different slopes than in 2D (figures not shown).

   To illustrate the effect of parallel transport on shapes (represented as a group of points) we compute the geodesic evolution between a circle and an ellipse with small anisotropy using LDDMM. The resulting initial momentum is then parallel
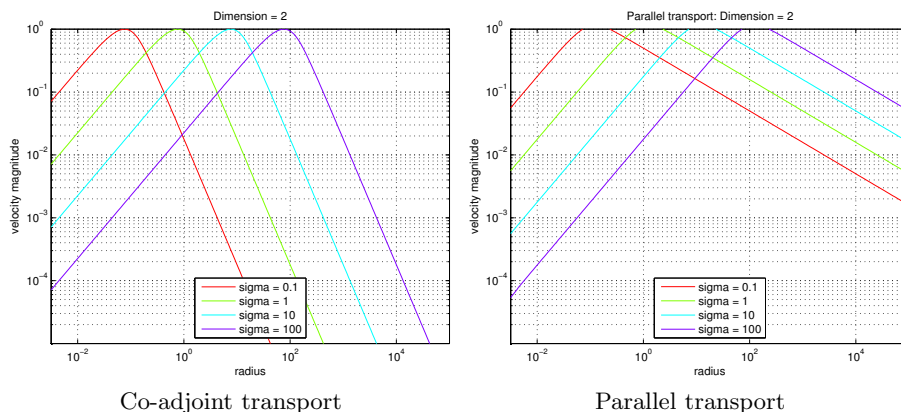
Co-adjoint transport   Parallel transport

Fig. 1. Co-adjoint and parallel transport for a 2D circular example for varying kernel sizes. Double-logarithmic plot (velocity magnitude over radius). A clear dependence of the velocity on the kernel size is observed. Maximal velocity normalized to 1 for comparison. Results were obtained using recursive adaptive Simpson quadrature.

transported along a geodesic mapping the initial circle to a smaller circle. Fig. 2 shows the used shapes and the result of evaluating the exponential map at time 1. From a geometric point of view it would be desirable to retain the anisotropy of the resulting ellipse at $t = 1$. However, LDDMM-based parallel transport clearly distorts the geometry and results in a much more circular shape: the ratio between the biggest and smallest axes decreases from 1.25 to 1.18.
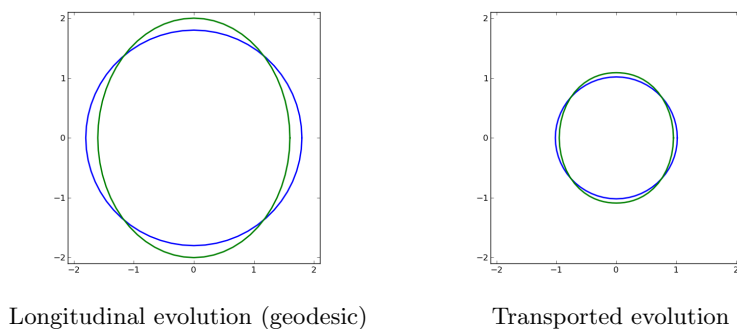

Longitudinal evolution (geodesic)   Transported evolution

Fig. 2. Left: 60 points on a circle are matched via a geodesic onto an ellipse with small anisotropy. Right: the transported evolution on a smaller circle: The anisotropy is distorted.
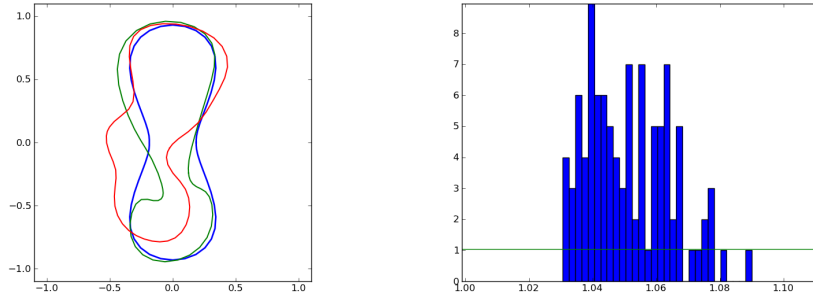
Fig. 3. Left: two random shapes in red and green and the blue template. Right: histogram of transported volume changes.

Last, we show an experiment illustrating the scaling issue when using parallel transport for population studies under the LDDMM metric: consider a population of closed curves drawn from a Gaussian model on the initial momentum around a template shape as shown in Fig. 3. Each shape of the population undergoes a small longitudinal change which is a uniform scaling centered on its barycenter. The population is separated into two groups, the first group has a scale evolution of 1.04 and the second group of 1.06. Hence, when looking at volume variation *alone*, the population clearly separates into two groups using a Gaussian Mixture Model (GMM) for instance. However, GMM completely fails to distinguish between the population when applied to the transported volume change. The histogram of the transported volume changes is given in Fig. 3.

These experiments motivate the need for a metric invariant to scale. Ideally, this should be accomplished by LDDMM to allow building on all its theory. Unfortunately, this cannot be achieved as described in the following Sec. 3.

3   Scale invariance and LDDMM geodesic flow

In Sec. 2 we observed that co-adjoint and parallel transport may exhibit counter-intuitive behavior under scaling using a Gaussian kernel. In this section, we show that the non-linear scaling effect is unavoidable when working with LDDMM, whatever the choice of the right-invariant metric.

We consider a group G of diffeomorphisms of the Euclidean space $\mathbb{R}^n$ which may or may not contain a group of diffeomorphisms denoted by G_0 that will represent the scaling transformations for instance. The first attempt to have scale invariance in the LDDMM framework is to ask whether we can design a kernel that defines a metric producing a global invariance of the flow of geodesics. Let us assume that G_0 contains the group of scaling transformations: $x \in \mathbb{R}^n \mapsto \lambda x$ for $\lambda \in \mathbb{R}^*_+$, but it may include more transformations such as translations and

rotations. The LDDMM framework is built on a group with a right-invariant distance that acts on the left on the space of shapes. It then induces a Riemannian metric on each orbit. A priori, requiring scale invariance for the induced metric is less demanding than asking it on the group itself. However, let us first explore the case of scale invariance on the group:

Definition 1 *The geodesic flow is invariant under G_0 if for any geodesics $t \mapsto \phi(t)$ the curve $t \mapsto g_0 \, \phi(t) \, g_0^{-1}$ is also a geodesic.*

Remark 31 *This definition implies the following fact: if (q_0, q_1) are two objects connected by the geodesic $q(t)$ then $g_0 \cdot q(t)$ is a geodesic connecting $(g_0 \cdot q_0, g_0 \cdot q_1)$.*

Theorem 32 *There does not exist any smooth right-invariant metric on the group of diffeomorphisms of $\mathbb{R}^n$ for which the geodesic flow is invariant under G_0 that contains rotations, translations and the scaling transformations.*

Proof. Let us consider a geodesic path $\phi(t)$ whose vector field is denoted by $v(t)$. By Ad invariance the vector field associated with $g_0 \phi(t) g_0^{-1}$ is $u(t) := \mathrm{Ad}_{g_0}(v(t))$. In addition to that, we know that $\phi(t)$ is a geodesic on the group if and only if it satisfies the Euler-Poincaré equation which is

$$\dot{m}(t) + \mathrm{ad}^*_{v(t)} \, m(t) = 0 \,, \tag{7}$$

where $m(t) = Lv(t)$ (or $v(t) = Km(t)$). Equivalently, we have

$$\dot{v}(t) + K \, \mathrm{ad}^*_{v(t)} \, Lv(t) = 0, \;\; \mathrm{Ad}_{g_0}(\dot{v}(t)) + K \, \mathrm{ad}^*_{u(t)} \, Lu(t) = 0.$$

This implies that

$$\mathrm{Ad}_{g_0}^{-1}(K \, \mathrm{ad}^*_{\mathrm{Ad}_{g_0} v(t)} \, L \, \mathrm{Ad}_{g_0} \, v(t)) = K \, \mathrm{ad}^*_{v(t)} \, Lv(t) \,, \tag{8}$$

which is, taking the dual pairing with $\omega \in V^*$ and using the Ad invariance:

$$\left(\mathrm{ad}_{\mathrm{Ad}_{g_0} v(t)} \, K \, \mathrm{Ad}_{g_0}^{-1*} \, \omega, L \, \mathrm{Ad}_{g_0} \, v(t) \right) = \left(\mathrm{ad}_{v(t)} \, K\omega, Lv(t) \right) \,.$$

$$\mathrm{ad}_{\mathrm{Ad}_{g_0} v(t)} \, K \, \mathrm{Ad}_{g_0}^{-1*} \, \omega = \mathrm{Ad}_{g_0} \left(\mathrm{ad}_{v(t)} \, \mathrm{Ad}_{g_0}^{-1} \, K \, \mathrm{Ad}_{g_0}^{-1*} \, \omega \right) \,.$$

Therefore, we have:

$$\left(\mathrm{ad}_{v(t)} \, \tilde{K}\omega, \tilde{L}v(t) \right) = \left(\mathrm{ad}_{v(t)} \, K\omega, Lv(t) \right) \,, \tag{9}$$

where $\tilde{K} = \mathrm{Ad}_{g_0}^{-1} \, K \, \mathrm{Ad}_{g_0}^{-1*}$ and $\tilde{L} = \tilde{K}^{-1}$. Hence, the Levi-Civita connections respectively associated with the right-invariant metrics K and $\tilde{K}$ are the same.

Let g_2 and $\tilde{g}_2$ denote the induced Riemannian metric on the space of two landmarks. The two metrics have the same geodesic equations and the same parallel transport. Since the two metrics are invariant w.r.t. translations and rotations, each kernel induces a metric on the landmark space on the real line that have the same geodesic equations. Let $L_{2,1}$ denote the manifold of 2 landmarks on $\mathbb{R}$, which is of dimension 2 and let $x \in L_{2,1}$ be a given point.

Let us first notice that the sectional curvature of the metric is given in page 80 of [5],

$$\kappa(r) = \frac{\gamma(0) - \gamma(r)}{\gamma(0) + \gamma(r)} \gamma''(r) - \frac{2\gamma(0) - \gamma(r)}{(\gamma(0) + \gamma(r))^2} [\gamma'(r)]^2 \,, \tag{10}$$

where r denotes the distance between the two landmarks. The second term is non positive and a simple argument will show that the first term is negative at some point: The function γ is positive and decreasing and cannot be constant (due to the positivity of the kernel); this implies that γ is not concave (otherwise its limit in $+\infty$ would be $-\infty$) so that there exists $x_0 \in \mathbb{R}_+^*$ such that $\gamma''(x_0) < 0$. Therefore, at this point x_0, $\kappa(x_0) < 0$.

Up to a scaling factor, we can assume that the two metrics coincide at a given vector in $v \in T_x L_{2,1}$. Since parallel transports coincide, it implies that the two metrics coincide on the image of v under the holomy group of v. In order to conclude that the two metrics are equal, we note that the holonomy group of $L_{2,1}$ has no non-trivial invariant subspaces: If it were the case, the metric would be decomposable by the De Rham decomposition theorem as a product of two one-dimensional spaces. As a consequence, the curvature should vanish everywhere.

This equality (up to a scaling factor $\alpha > 0$) evaluated on Dirac distributions gives:

$$\left(\mathrm{Ad}_\lambda^{-1*} \delta_x^{p_x}, K \, \mathrm{Ad}_\lambda^{-1*} \delta_y^{p_y} \right) = \alpha \left(\delta_x^{p_x}, K \delta_y^{p_y} \right) . \tag{11}$$

Finally, using the fact that $\mathrm{Ad}_{g_0}^{-1*} \delta_x^{p_x} = \delta_{\lambda x}^{p_x/\lambda}$ when $g_0 : x \mapsto \lambda x$, we get:

$$\lambda^2 \langle p_x, K(x,y) p_y \rangle = \alpha \langle p_x, K(\lambda x, \lambda y) p_y \rangle , \tag{12}$$

and therefore: $\lambda^2 K(x,y) = \alpha K(\lambda x, \lambda y)$ for all $\lambda \in \mathbb{R}_+^*$. In particular, letting $\lambda \to 0$, we obtain, using the continuity of K, $K(0,0) = 0$ which is not a positive symmetric matrix. This is a contradiction. $\square$

Remark 33 *If the kernel were not required to be continuous, a possible solution would be the Dirac kernel $\delta_{x,y}$. Such metrics are known to be degenerate [1].*

Hence, it is necessary to go beyond the standard LDDMM framework to obtain scale invariance. Our interest in scale invariance was only motivated by the study of parallel transport and its global and local effects. In Sec. 4, we characterize Riemannian metrics with invariance of a global indicator under parallel transport.

4 Designing Riemannian metrics

4.1 Decomposition theorem

Let us assume that we aim at preserving the volume variation in longitudinal evolutions, which is of interest in the case of Alzheimer's disease. In more mathematical words, the volume variation must be preserved under parallel transport. We will restrict ourselves to the space of shapes that are described as embeddings of the unit circle S_1 in $\mathbb{R}^2$ or sphere embeddings in $\mathbb{R}^3$. We would like to distinguish between local shape variation and global volume change. Although the two quantities are strongly linked in general situations, it seems quite reasonable to assume a uniform volume change. A natural approach to distinguish between volume variation and shape (up to scaling) variation is to decompose the space of shapes (in the spirit of [10]) using the following map:

$$\mathrm{Emb}(S_1, \mathbb{R}^2) \mapsto \mathbb{R}_+^* \times \mathrm{Emb}_1(S_1, \mathbb{R}^2); \quad s \to (\mathrm{vol}(s), P(s)) ,$$

where vol is the surface delimited by the closed curve s and P is a chosen projection on the space of unit surface embeddings denoted by $\mathrm{Emb}_1(S_1, \mathbb{R}^2)$. A product between the standard Euclidean metric on $\mathbb{R}_+$ and a metric on the space $\mathrm{Emb}_1(S_1, \mathbb{R}^2)$ gives a (Riemannian) metric on the shape of space that meets our requirement: Namely, that the volume variation is invariant w.r.t. parallel transport. Using the de Rham decomposition theorem, it turns out that this is the only possible sort of metric that fulfills this invariance condition. The following result is a particular case of the De Rham decomposition theorem and we give a proof for completeness (see [8] for a proof in the general case).

Theorem 41 *Let g be a Riemannian metric on a connected Riemannian manifold M and a surjective function $f : M \mapsto \mathbb{R}$ such that $df(x) \neq 0$ for all $x \in M$ and which is invariant under parallel transport, i.e. $\nabla df = 0$, then (M, g) can be decomposed into a direct product of Riemannian metrics as follows:*

$$(M, g) = (\mathbb{R}, dt^2) \times (M_0, g_0) \tag{13}$$

where g_0 is a Riemannian metric on the submanifold $M_0 := f^{-1}(\{0\})$.

Proof. Let us first introduce the notation V being the unit length vector field associated with df via the metric g. In other notations, one has $V = df^\sharp$. In particular, if $Y \in T_{x_0} M_0$ then $\langle V, Y \rangle = df(Y) = 0$. It is easy to prove that the following mapping is a global diffeomorphism:

$$\Psi : \mathbb{R} \times M_0 \mapsto M; \quad (t, x_0) \mapsto \exp_{x_0}(tV(x_0)), \tag{14}$$

where $\exp$ denotes the Riemannian exponential. Indeed, since

$$\nabla_X V = 0 \ \forall X \in \chi(M), \tag{15}$$

we get $\nabla_V V = 0$ so that V is a geodesic vector field. In addition, for every vector field X, we have $R(V, X)V = \nabla_V \nabla_X V - \nabla_X \nabla_V V - \nabla_{[V,X]}V = 0$ so that the Jacobi field equation for a vector $J(x_0) \in T_{x_0} M$ reduces to $\frac{D^2 J}{dt^2} + R(V, J)V = \frac{D^2 J}{dt^2} = 0$.

Hence, the map (14) is a local diffeomorphism, which is obviously an injection so that this is a global diffeomorphism. Now, let us denote by X, Y two vector fields on M_0 trivially extended on M via the diffeomorphism Ψ. Namely, for each $t \in \mathbb{R}^*$, one defines $(t, x) \mapsto \psi_*(t)X(x)$ and $(t, x) \mapsto \psi_*(t)Y(x)$ the natural extensions of X and Y. One has $\psi_*(t)[X, Y] = [\psi_*(t)X, \psi_*(t)Y] = 0$. By construction, we also have $V(t, x_0) = \psi_*(t)V(0, x_0)$ so that this implies that $[X, V] = [Y, V] = 0$. Using $[X, V] = 0 = \nabla_X V - \nabla_V X$, and equation (15), we get $\nabla_V X = 0$. In particular, the equality

$$V \cdot g(X, Y) = g(\nabla_V X, Y) + g(X, \nabla_V Y) = 0$$

holds which means that the pull-back of the metric g by Ψ is $dt^2 + g_0$. $\square$

Remark 42   – *This result is valid in finite dimension and might remain valid in a smooth infinite dimensional context. In applications however, shapes are approximated in high-dimensional spaces and the theorem does apply. Proving a convergence theorem (when the dimension increases) goes beyond the scope of the paper.*
  – *The theorem can be generalized to k functions. The condition on the differentials would be that the family $(df_1(x), \dots, df_k(x))$ is linearly independent.*

4.2   An induced Riemannian metric

To design a metric following the theorem, we therefore need a Riemannian metric on the space of unit volume shapes. To this end, one can use the restriction of any Riemannian metric on the space of volume preserving embeddings. Since we based our discussion on the LDDMM metric, we consider the Riemannian metric induced by LDDMM on that submanifold and we now present the geodesic computation for the LDDMM metric with a volume constraint.

We denote by V an admissible RKHS of vector fields (see [15]). Let $q \in \mathrm{Emb}_1(S_1, \mathbb{R}^2)$ be an embedding of surface of volume 1, we consider the set of vector fields $V_q := \{v \in V \mid d\operatorname{vol}_q(v(q)) = 0\}$. Since V is a RKHS of admissible vector fields, $v \to d\operatorname{vol}_q(v(q))$ is a continuous linear form and its kernel V_q is a closed subspace of V. Note that the notation $d\operatorname{vol}_q$ stands for the differential of the volume at point q which is a linear form on the tangent space $T_q \mathrm{Emb}(S_1, \mathbb{R}^2)$. We denote by π_q the orthogonal projection on $\operatorname{Ker} d\operatorname{vol}_q$ for the L^2 scalar product on $L^2(S_1, \mathbb{R}^2) \simeq T_q \mathrm{Emb}(S_1, \mathbb{R}^2)$.

A geodesic between two elements $q_0, q_1 \in \mathrm{Emb}_1(S_1, \mathbb{R}^2)$ is a solution of

$$\inf \int_0^1 \|v(t)\|_{V_{q(t)}}^2 \, dt \,, \tag{16}$$

under the constraints $\dot{q} = v(t)(q)$ where $v(t) \in V_{q(t)}$ and $q(0) = q_0$ and $q(1) = q_1$.

Proposition 1 *The minimization problem* (16) *can be recast into:*

$$\inf \int_0^1 \|v(t)\|_V^2 \, dt \,, \tag{17}$$

under the constraint $\dot{q} = \pi_q(v(t)(q))$ *where* $v(t) \in V$ *and* $q(0) = q_0$ *and* $q(1) = q_1$.

Proof. Clearly, Problem (16) is contained in Problem (17), since $v(t) \in V_{q(t)}$ implies $\pi_q(v(t)(q(t))) = v(t)(q(t))$. Let $v(t)$ be an optimal solution of Problem (17), then denoting $\pi_q : V \mapsto V_q$ the orthogonal projection, we get:

$$\int_0^1 \|\pi_q(v(t))\|_V^2 \, dt \leq \int_0^1 \|v(t)\|_V^2 \, dt \,.$$

Therefore, we have $\pi_q(v(t)) = v(t)$ which is a solution of Problem (16). $\square$

Using an optimal control approach, the optimal solutions of Problem (17) are given by the solutions of the Hamiltonian equations

$$\begin{cases} \dot{q} = \partial_p H(p, q) \\ \dot{p} = -\partial_q H(p, q) \,, \end{cases} \tag{18}$$

where the Hamiltonian function is given by $H(p, q) = \frac{1}{2}\langle \pi(p), K(q)\pi(p) \rangle$; $K(q)$ is the kernel matrix associated to the LDDMM metric at point q.

4.3   The choice of projection

A geodesic on the space of shapes can then be decomposed into a straight line on the volume axis and a geodesic on the submanifold of unit volume shapes. In the previous section, we have defined the metric on the space of unit volume shapes. It remains to define the volume geodesics. As mentioned in remark 42, the range of choice of projection may be large and it is natural to impose additional assumptions such as invariance w.r.t. translations, i.e. $P(T(m)) = T(P(m))$ for every translations T in $\mathbb{R}^n$. This is still not sufficiently constrained to uniquely determine the metric. Scaling invariance around the barycenter of the shape defined by $m(s) := \int_S c(s)ds = 0$ uniquely defines the projection: scale invariance means $P(\lambda m) = P(m)$ for every $\lambda \in \mathbb{R}_+^*$ for a centered (at 0) shape m. This is the first metric we will consider in the experiments.

The notion of scale invariance also depends on the definition of the center of the shape which may be unnatural for some shapes. In order to avoid such a bias, we also propose to define the projection using the gradient flow of the volume with respect to a given metric, for instance the LDDMM metric: indeed, if f is a real function defined on a manifold M with no critical points, then the vector field ∇f is non-vanishing on M and defines the volume geodesics. However, the gradient is defined by the choice of a metric on the tangent space: for instance, an LDDMM type of metric which provides spatial correlation. This defines the second metric in our experiments.

5   Experimental Results

We compare LDDMM and the volume/shape-decoupled model represented by the two metrics introduced in Sec. 4.3. We use the Schild's ladder method to compute parallel transport. Fig. 4 illustrates the effect of the non-preservation of volume variation with the standard LDDMM metric even if template and target volumes and scales are equivalent. This shows that volume variation transport is already affected by shape deformations at the same scale. We use 60 landmarks and a Gaussian kernel of standard deviation 0.1 for the simulation. The volume variation for the LDDMM transported evolution is 1.06 whereas the initial data shows a volume variation of 1.104. By construction, for the new metrics, the volume variation is the same for the transported evolution. However, since the projections are different, the two different final curves in red and green are distinct. The last experiment illustrates the difference between the two new metrics, where the second metric uses a Gaussian kernel of width 0.01 in the definition of the volume gradient. We perform parallel transport of the longitudinal evolution shown in Fig. 4 (upper left) on the blue curve (bottom right). The transported evolutions exhibit very different behavior: the green curve is the transport using the scale invariant metric and shows that in some parts of the shape there is no local growth, whereas the other metric (represented by the red curve) offers a more uniform growth pattern on the shape.
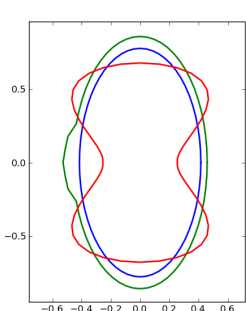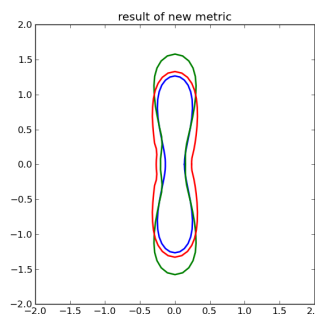
Longitudinal evolution, target shape in red
(a scaling composed with a bump).
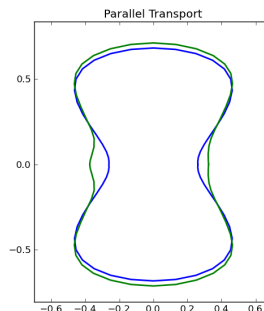
Transported evolution
LDDMM with Gaussian kernel $\sigma = 0.1$.
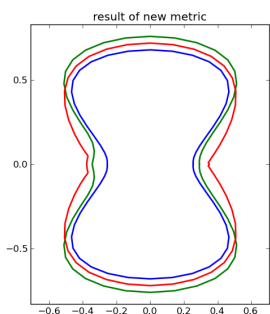
Transported evolutions under the scale invariant
metric in green and the other metric in red.

Difference between the two metrics.

Fig. 4. Examples of parallel transport under the new metrics.

6   Conclusions and Future Work

This paper explored the behavior of parallel transport for the LDDMM regis-
tration model. We showed that LDDMM is never scale invariant and does not
conserve global properties such as absolute or relative volume changes. To achieve
preservation of global properties we developed a new set of Riemannian metrics
and demonstrated their behavior in comparison to the standard LDDMM model.
While this paper so far only scratched the surface of metric design to achieve
desired properties under parallel transport it raises fundamental issues for the
analysis of longitudinal shape and image data when moving beyond global in-
dicators. Future work will consist in estimating the statistical gain (e.g., w.r.t.
LDDMM) when using the proposed metrics on a particular data set of biomedical
shapes where a global indicator already achieves good performance.

References

1. Bauer, M., Bruveris, M., Harms, P., Michor, P.: Geodesic distance for right invariant Sobolev metrics of fractional order on the diffeomorphism group. Annals of Global Analysis and Geometry pp. 1–17 (2012)
2. Beg, M., Miller, M., Trouvé, A., Younes, L.: Computing large deformation metric mappings via geodesic flows of diffeomorphisms. IJCV 61(2), 139–157 (2005)
3. Fiot, J.B., Risser, L., Cohen, L.D., Fripp, J., Vialard, F.X.: Local vs global descriptors of hippocampus shape evolution for Alzheimer's longitudinal population analysis. In: STIA. pp. 13–24 (2012)
4. Lorenzi, M., Ayache, N., Pennec, X.: Schilds ladder for the parallel transport of deformations in time series of images. In: IPMI. pp. 463–474. Springer (2011)
5. Micheli, M.: The Differential Geometry of Landmark Shape Manifolds: Metrics, Geodesics, and Curvature. Ph.D. thesis, Division of Applied Mathematics, Brown University (2008)
6. Muralidharan, P., Fletcher, P.: Sasaki metrics for analysis of longitudinal data on manifolds. In: CVPR. pp. 1027–1034. IEEE (2012)
7. Rao, A., Chandrashekara, R., Sanchez-Ortiz, G., Mohiaddin, R., Aljabar, P., Hajnal, J., Puri, B.K., Rueckert, D.: Spatial transformation of motion and deformation fields using nonrigid registration. IEEE TMI 23(9), 1065–1076 (2004)
8. Sakai, T.: Riemannian geometry. Transl. from the Japanese by Takashi Sakai. Translations of Mathematical Monographs. 149. Providence, RI: American Mathematical Society (AMS). 358 p. (1996)
9. Singh, N., Fletcher, P., Preston, J., Ha, L., King, R., Marron, J., Wiener, M., Joshi, S.: Multivariate statistical analysis of deformation momenta relating anatomical shape to neuropsychological measures. MICCAI pp. 529–537 (2010)
10. Sundaramoorthi, G., Mennucci, A., Soatto, S., Yezzi, A.: A new geometric metric in the space of curves, and applications to tracking deforming objects by prediction and filtering. SIAM Journal on Imaging Sciences 4(1), 109–145 (2011)
11. Sundaramoorthi, G., Mennucci, A., Soatto, S., Yezzi, A.: A new geometric metric in the space of curves, and applications to tracking deforming objects by prediction and filtering. SIAM J.also Imaging Sciences (2011)
12. Sundaramoorthi, G., Yezzi, A.J., Mennucci, A.C.: Properties of Sobolev-type metrics in the space of curves. Interfaces and Free Boundaries, European Mathematical Society , 10(4), 423–445 (,2008)
13. Twining, C., Marsland, S., Taylor, C.: Metrics, connections, and correspondence: the setting for groupwise shape analysis. In: Energy Minimization Methods in Computer Vision and Pattern Recognition. pp. 399–412. Springer (2011)
14. Vaillant, M., Miller, M., Younes, L., Trouvé, A., et al.: Statistics on diffeomorphisms via tangent space representations. NeuroImage 23(1), 161 (2004)
15. Younes, L.: Shapes and diffeomorphisms, vol. 171. Springer (2010)
16. Younes, L., Michor, P., Shah, J., Mumford, D.: A metric on shape space with explicit geodesics. Atti Accad. Naz. Lincei Cl. Sci. Fis. Mat. Natur. Rend. Lincei (9) Mat. Appl. 19(1), 25–57 (2008)
17. Younes, L., Qiu, A., Winslow, R., Miller, M.: Transport of relational structures in groups of diffeomorphisms. Journal of mathematical imaging and vision 32(1), 41–56 (2008)